PAPER • OPEN ACCESS

Numerically optimized band boundaries of Planck mean absorption coefficients in air plasma

To cite this article: P Kloc *et al* 2017 *J. Phys. D: Appl. Phys.* **50** 305201

View the article online for updates and enhancements.

IOP ebooks™

Bringing you innovative digital publishing with leading voices to create your essential collection of books in STEM research.

Start exploring the collection - download the first chapter of every title for free.

Numerically optimized band boundaries of Planck mean absorption coefficients in air plasma

P Kloc, V Aubrecht and M Bartlova

Centre for Research and Utilization of Renewable Energy, Faculty of Electrical Engineering and Communication, Brno University of Technology, Technicka 10, 61600 Brno, Czechia

E-mail: klocpetr@feec.vutbr.cz

CrossMark

Abstract

Radiation heat transfer plays an important role in the energy balance of plasma in an electric arc and its accurate prediction is essential for the development of new electrical devices. Unfortunately, a very complex spectrum of the absorption coefficient makes accurate radiation heat transfer calculations a very challenging task, especially with complex geometries. Numerical approximation of the absorption coefficient is therefore commonly used to reduce computing demands. This paper presents our contribution to the topic of computing requirements reduction, namely the problem of frequency band selection for mean absorption coefficients (MACs). We show that, with the proper band distribution and averaging method, even a very low number of bands can be sufficient for an accurate approximation of the real radiation heat transfer. The band selection process is based upon numerical optimization with a mean value of each band being calculated as a line limited Planck MAC. Both the line limiting factor and associated characteristic plasma absorption length are investigated in detail and an optimal value equal to the three plasma radii is proposed. Tables for three bands mean absorption coefficients in air at the pressure of 1 bar and temperature range spanning from 300 K to 30 kK are included in this paper. These tables serve as input parameters for a fast evaluation of radiation transfer using either the P1 or discrete ordinates method (DOM) approximation with satisfactory accuracy.

Keywords: radiation, radiative heat transfer, arc, air, mean absorption coefficient, band average, numerical optimization

(Some figures may appear in colour only in the online journal)

1. Introduction

Radiation transfer plays an important role in many plasma processes and thus cannot be omitted in relevant numerical simulations. However, physically unreasonable results can be obtained without an accurate radiation transfer evaluation [1]. Unfortunately, accurate radiation transfer evaluation is not an easy task, as the long range nature of radiation propagation makes a spatial model very computationally demanding. This, coupled with the spectral resolution required for an accurate description of the spectrum, creates a very complex computational problem.

Several approaches have been historically used to simplify the radiation transfer calculations. The oldest and still quite widespread method is the net emission coefficients (NEC) [2]. This method simplifies both the spatial and spectral parts of the radiation transport problem. It is very easy to implement with the requirement of the plasma radius and temperature as input parameters only for a given plasma composition. The absorption coefficient spectrum is required for the estimation

J. Phys. D: Appl. Phys. **50** (2017) 305201

P Kloc *et al*

of NEC. However, this can be done in advance and the value of NEC is often tabulated for given plasma parameters. The drawback is in applicability, as this method can reliably predict radiation losses only in the hottest, central regions of the plasma. It does not describe the radiation reabsorption in the colder regions and thus cannot evaluate the amount of radiation escaping the plasma.

The partial characteristics (PC) [3] method is more complex, but it solves both the spatial and spectral parts of the radiation transfer in one compact calculation. Unlike NEC, this method includes the calculation of the radiation transfer in the absorbing parts and, therefore, can predict the amount of radiation escaping the plasma. This method has not seen much widespread usage, as it relies on a very large database, which makes it difficult to use for more complex problems, especially ones with pressure gradients.

Finally, a quite commonly used approach relies on the independent solution of both the spatial and spectral part of the radiation transfer. This approach allows the development of a separate method for each task. Discrete ordinates method (DOM) or P1 approximations are widely used for numerical calculations of the spatial part [5] but operate only with a single value of the absorption coefficient. An approximation in the spectral part then comes from a reduction in the number of required frequency intervals. This stems from the fact that the number of intervals for accurate description of the spectrum [4] is in the order of 10^5. The numerical reduction consists of the calculation of an effective value for just a few frequency intervals or frequency bands. Even a single band spanning the entire frequency range can be used in the most extreme cases and the approximation is then called '*grey model*'.

Proper handling of the bands distribution and calculation of the effective value inside each band plays a critical role in the overall accuracy of the approximation method. Quite often, the effective value within each band is calculated as some form of mean value of the absorption coefficient inside that band. Generally, two mean values are used in the literature: either the Planck or the Rosseland mean absorption coefficient (MAC) [5]. In the case of the Planck MAC, a line limiting procedure is usually applied in order to limit the inherent line overestimation and to increase the accuracy [6].

The selection of the bands distribution has a critical influence on accuracy. Yet, there is no clear guideline available how to define these intervals. Peyrou [7] gives the advice only that the absorption coefficient should not vary strongly within one band. Nordborg and Iordanidis [6] used the variation of the spectral absorption coefficient with the temperature as the base for the band selection. Hannachi *et al* [10] grouped the absorption coefficients into bands based on the energies and important processes in the considered mixture, while Jan *et al* [8] based their band distribution on the variation of the absorption continuum. Reichert *et al* [9] successfully used a 7-band MAC radiation model in a commercial CFD program, but unfortunately did not state the method they used for the band selection. It is thus clear that proper band selection is a very complex task.

One way to ensure the optimal band selection is an employment of numerical optimization. Fagiano and Gati [11]

proposed a method for numerical optimization of both the band distribution and the effective value inside each band. This method could be probably the most accurate approximation in case of particular plasma composition and its temperature profile. The problem is that each temperature profile may result in a unique band distribution, as well as effective values inside each band, as suggested in [16]. This effect limits the applicability of full optimization for general usage.

In this paper we try to find some middle ground between full optimization and no optimization. We calculated the effective value inside each band as a line limited Planck MAC, while calculating the optimal band distribution with a numerical optimization code. We decided to limit ourselves to the case of air at the pressure of 1 bar and limit the number of bands to three for several reasons. Namely, air plasma is typical for many low voltage devices, such as switch gears or circuit breakers, and having reliable MACs for the fast radiation evaluation would be convenient. Furthermore, the low number of frequency bands contributes to the fast evaluation and low computing power requirements.

Reducing the number of bands is aimed at highlighting the most important band boundaries. If the position of the band boundaries can be traced to some important feature in the absorption coefficients, then it might be possible to estimate the optimal band distribution in the future even without an optimization procedure.

In this paper, we focus on the divergence of radiation flux as the mean to evaluate the MACs accuracy. It is arguably the best quantity to represent the radiation energy balance inside the thermal plasma. Other quantities, such as radiation flux, might not be represented as accurately. However, the entire process is quite adaptable and it is possible to use radiation flux or even a weighted mean of radiation flux and divergence of radiation flux as an objective function for the optimization. The question of optimal objective function goes beyond the scope of this paper.

2. Model and its input parameters

The basic idea behind the model is quite straightforward and can be described in a series of simple steps. First, we defined our calculation domain as an infinitely long cylinder with an arbitrary temperature profile. Several different sets of the temperature profiles were used to investigate the general temperature profile impact on the optimal band selection. Each set of temperature profiles consists of three temperature profiles, defined with the same core and outer temperature, but with different general shapes. The difference between the sets lies in the value of the core temperature, which is varied between 5 kK and 25 kK. An example of two different sets of temperature profiles is shown in figure 1. All of the temperature profiles from all of the sets are produced using the same formula given as

$$T(r) = T_{\max} - (T_{\max} - T_{\min})\frac{1 - \exp(-n(r/R)^3)}{1 - \exp(-n)}, \quad (1)$$

where $T_{\max}$ and $T_{\min}$ are the maximum and minimum temperatures respectively, $R = 1\,\text{cm}$ is the selected size of the domain and n is a free parameter, specifying the profile shape.
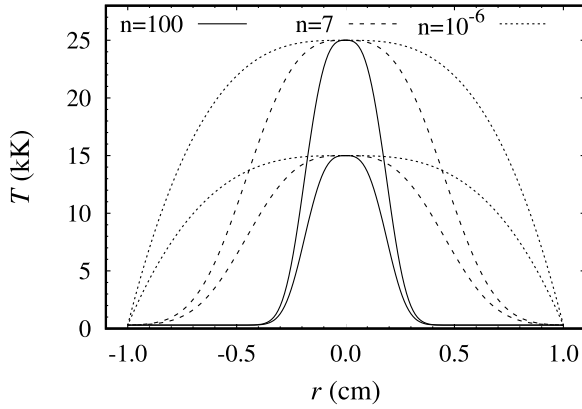
Figure 1. An example of temperature profiles used in the calculations. Two sets with different core temperature are shown.
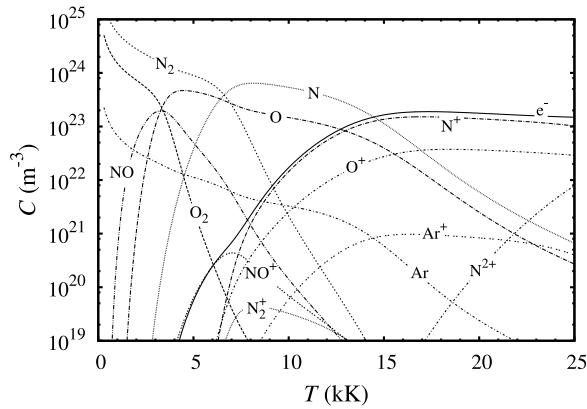

Figure 2. Composition of air plasma at 1 bar as a function of the temperature.

We assumed the cylinder to be filled with 1 bar of air with the composition given in figure 2. Plasma composition was calculated according to [13] with input parameters taken from [14]. We assume the LTE criterion to be fulfilled everywhere in the domain and, for each temperature, calculate the absorption coefficient according to [12], which includes the contribution of N_2, O_2, NO, NO_2 and N_2O molecular species and their relative ions, as well as O, N and Ar atomic species up to the third ionization level. The only difference is that we used Voigt line profile approximation given by Whiting [15].

For each temperature profile, we calculated the divergence of the radiation flux in 20 points evenly distributed along the cylinder radius. The calculation is carried for full 3D angular discretization of the radiation with eight azimuthal and three polar directions in one hemisphere. This divergence of radiation flux serves as the base for the optimization procedure in later steps and is referred to as the '*exact*' divergence of radiation flux in this paper. The number of spatial points in which the divergence of the radiation flux were evaluated were not chosen randomly. We wanted the exact profile to be represented quite accurately, while keeping the comparison process defined below as fast as possible. With 20 points, both requirements are reasonably satisfied, as shown in figure 3. Additional points would indeed improve the accuracy of the representation, but would lead to the notable increase in the
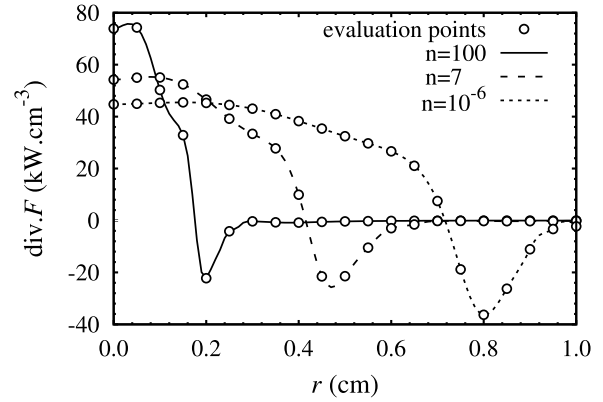

Figure 3. Divergence of radiation heat flux along the infinitely long cylinder radius for the three different temperature profiles. The temperature in the cylinder center was 25 kK in all cases. The circles mark the position of the points selected for calculation of the norm in (2).

calculation time and would not provide any benefit to the optimization procedure.

To evaluate the difference between the exact divergence of radiation and the value obtained by using the mean absorption coefficients (MACs) we defined a norm as

$$\Delta F = \frac{1}{20}\sqrt{\sum_{i=1}^{20} \alpha_i (\nabla \cdot \boldsymbol{F}_{\text{ex},i} - \nabla \cdot \boldsymbol{F}_{\text{MAC}_\nu,i})^2}, \qquad (2)$$

where α_i is the weight of the *i*th point. In this paper, we kept the weight $\alpha_i = 1$ for all of the points *i*, thus keeping the weight constant across the entire cylinder radius. The areas where the value of the exact divergence of radiation flux is further away from zero therefore plays a more important role in an accuracy evaluation.

The norm defined in (2) provides an excellent target function for numerical optimization. Unfortunately, it is not best suited for a presentation of the results as the absolute value depends strongly on the core temperature and total amount of radiation. For presentation purposes, it is better to express the norm as a relative quantity. We divided the norm defined in (2) by a factor corresponding to the absolute value of the exact divergence of the radiation flux

$$\Delta F' = \Delta F \left(\frac{1}{20}\sum_{i=1}^{20} |\nabla \cdot \boldsymbol{F}_{\text{ex},i}| \right)^{-1} \qquad (3)$$

and use this reduced norm for presentation purposes. Even though this expression does not exactly describe the relative error, it is easier to understand than the absolute values as defined in (2).

We proceeded to construct a frame for the calculation of MACs for the given temperature profile, following the calculation of the exact divergence of radiation flux. We decided to use a 3 bands model for its fast interpretation. This is indeed a very low number of bands, but we wanted to show that, with the correct optimization procedure, this number is sufficient to produce quite accurate results. It is also advantageous for more complex plasma calculations to reduce the burden of

J. Phys. D: Appl. Phys. **50** (2017) 305201

P Kloc *et al*

radiation calculation by considering as few spectral bands as possible.

The MAC value inside each band was calculated using a Planck average. This average is known to overestimate the importance of high values of the absorption coefficient, namely atomic lines. To mitigate this problem, we used the line limiting method proposed by Nordborg [6] and applied it to the atomic lines only. The absorption coefficient of atomic lines is replaced by

$$\kappa_{\text{lim}} = \frac{1}{L}(1 - e^{-\kappa_{\text{line}}L}) \tag{4}$$

with the total absorption coefficient calculated as the sum of molecular, atomic continuum and atomic lines contributions

$$\kappa = \kappa_{\text{mol}} + \kappa_{\text{cont}} + \kappa_{\text{lim}}. \tag{5}$$

This method requires knowledge of the characteristic absorption length L. We included the search for optimal characteristic absorption length into our optimization process. We assumed some fixed value of L and let the band optimization process (described below) to find the best band distribution. Then, we slightly increased the value of L and repeated the process. In this manner, we covered a reasonable range for each temperature profile and located the most accurate value of characteristic absorption length L.

A numerical optimization process was used to localize the best distribution of bands. With three bands, this represents a two dimensional global optimization problem with a target function defined in (2). From our earlier tests [16], we have found that the objective function can behave quite wildly, changing its value significantly over a very narrow frequency range corresponding to the atomic line width. This disqualifies large portion of the global optimization algorithms from being usable in this case. In the end, we decided to use an algorithm developed by Changton and Bo, which is based on a modified downhill simplex method [17]. This method is very easy to implement but does not guarantee finding the global optimum. We tried to tackle this issue by starting the optimization process several times, each time randomly selecting the initial pool of band boundaries. The initial pool size was 22 pairs of randomly generated band boundaries. If the algorithm converged to the same band distribution in a sufficient number of repetitions, we declared such a band distribution the global minimum for the given parameters.

Let us recapitulate the entire process once more for better clarity. For the sake of simplicity, we will describe the process for a single temperature profile only. First, we assume a fixed temperature profile and for that profile, we calculate the exact divergence of the radiation flux along the radius of infinitely long cylinder. The cylinder is assumed to be filled with air at pressure of 1 bar. Then, we define some small starting value of characteristic absorption length L and apply the *Nordborg line limiting factor*. Subsequently, we repeatedly ran the band distribution optimization process for three bands, finding the best band distribution corresponding to the chosen value of L. Finally, we repeat the process for different values of characteristic absorption length L.

3. Results and discussion

In the following three subsections, we discuss our handling of the calculation of the optimal characteristic absorption length, its role in calculation of the optimal band distribution and the accuracy of the mean absorption, respectively. The optimal values of MAC are then presented in the appendix. Note that the tables presented in the appendix were calculated for the air with a pressure of 1 bar only. Therefore, they are suitable for low pressure applications or devices which are open to the ambient air.

3.1. Characteristic absorption length

The line limiting factor has to be applied when employing Planck MACs, otherwise the atomic lines would be greatly overestimated, leading to an unrealistically large emission and absorption in the plasma core and outskirt, respectively. The line limiting factor is associated with a characteristic absorption length L. It is convenient to express this quantity in relation to some characteristic dimension of the plasma.

The characteristic absorption length and associated line limiting factor were derived for isothermal plasma in the original paper by Nordborg [6]. The plasma radius R_{p} is a well defined dimension in such a case and can be used as a reference value. Even in the original paper, it is suggested that characteristic plasma absorption length should be equal to the plasma diameter $L \approx 2R_{\text{p}}$.

The situation is a bit more complicated in the case of plasma with a temperature and/or pressure profile. The plasma radius is not clearly defined in such a case and many different definitions can be advocated. In this paper, we defined the plasma radius R_{p} as a distance from the cylinder axis, where the temperature reaches the half point between the maximum and minimum value. Considering the temperature profile definition in (1), one can express the plasma radius analytically as

$$R_{\text{p}} = \sqrt[3]{-\frac{1}{n}[\log(1 + \exp(-n)) - \log(2)]} \, R. \tag{6}$$

We used this definition of plasma radius because it is independent of both the core and the boundary temperature and is dependent only on the parameter n and domain size R. Even though it is hardly the best definition of plasma radius, it is advantageous for our purpose of testing several different sets of temperature profiles within fixed calculation domain. We will use this plasma radius as the reference value for evaluation of the characteristic absorption length.

It is worth noting that the optimal band distribution was not the same across the entire testing range of L. However, it does not mean that each tested characteristic absorption length resulted in a unique frequency band distribution. Rather, several unique band distributions can be observed in the entire testing range of the characteristic absorption length. Interestingly enough, changes in band distribution are not associated with any significant or unexpected change in the behaviour of the reduced norm $\Delta F'$. The profiles in figure 4 appear to be smooth without visible transitions from one
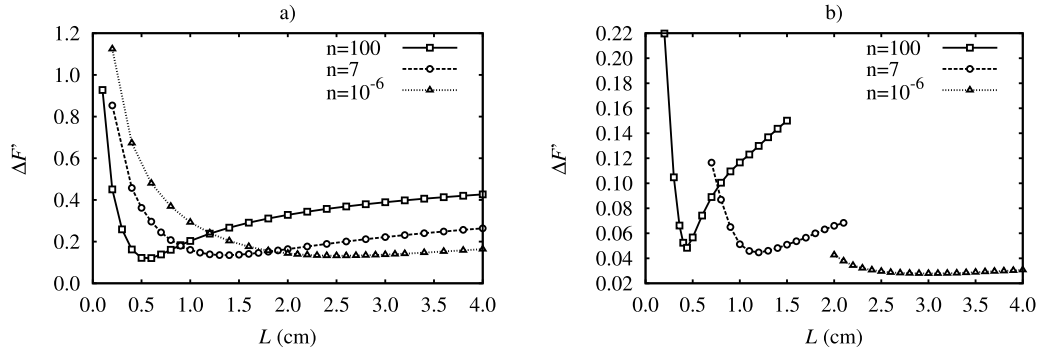
Figure 4. Dependence of the reduced norm expressing the approximation accuracy on the selected value of the characteristic absorption length L for different temperature profile shapes. Figures (a) and (b) were calculated for temperature profile core temperature 25 kK and 15 kK, respectively. Note that (a) and (b) are using different *y*-axis scales.

band distribution to another. This is likely caused by a very small approximation error between several band distributions. Using sub-optimal band distribution does not necessarily lead to significantly decreased accuracy.

The influence of the characteristic absorption length on the approximation accuracy is shown in figure 4. Two sets of temperature profiles with different core temperatures are presented. Two conclusions can be drawn from the reduced norm behaviour. Namely that a single value L_{best} exists for each temperature profile, which produces the most accurate approximation of the exact solution. The accuracy decreases as the value of characteristic plasma absorption length L moves further away from the most accurate value L_{best}. Such behaviour can be explained on the basis of the line limiting factor derivation in the original work. When the characteristic absorption length is too small, the line limiting is not sufficient and the vast overestimation of the unmodified Planck MAC takes over. On the other hand, overestimation of the characteristic absorption length leads to the assumption of a weaker radiation emission in the core and radiation trapping early in the plasma column.

The second conclusion can be drawn from the comparison of reduced norm behaviour for smaller and larger values of the characteristic absorption length, respectively. The reduced norm $\Delta F'$ rises much faster in the case of the lower values, in comparison with the larger ones. This is especially apparent in the case of $n = 100$ with very steep dependence on lower values of characteristic absorption length. Therefore, we conclude that it is much better to overestimate the characteristic absorption length rather than underestimate it.

The most accurate values of the characteristic plasma absorption length are summarized in table 1 for every tested temperature profile. Note that even profiles with the same shape factor n result in unique values. Such behaviour is preventing the inclusion of the characteristic absorption length evaluation into the numerical optimization procedure. Each case would require unique handling, and it would be nearly impossible to find generally applicable values of the characteristic absorption length L. However, it is possible to generalize the results with the method used in this paper and with the help of the second conclusion mentioned above. One can

Table 1. Obtained the most accurate characteristics plasma absorption length L_{best} (expressed as multipliers of plasma radius R_p which serves as the base unit) for various core temperatures and shape parameters n. The last line indicates the value of plasma radius for given profile parameter n.

T_{max} (kK)	$n = 100$	$n = 7$	$n = 10^{-6}$
25	2.94	2.96	3.18
20	3.25	3.29	3.51
15	2.26	2.60	3.75
10	2.00	2.47	2.85
R_p (cm)	0.19	0.46	0.79

come to the understanding that the generally applicable value of the characteristic absorption length should be $L \approx 3R_p$.

Indeed, this is a *rule of thumb* rather than a hard rule. Many fields in table 1 contain larger values, namely those for $T_{max} = 20$ kK and $n = 10^{-6}$. Nevertheless, the error induced by the not-optimal value of the characteristic absorption length varies very slowly for $n = 10^{-6}$ and is within 3% in the case of $T_{max} = 20$ kK. The declaration of the generalized optimal value of $L_{optim} = 3R_p$ is thus an acceptable compromise between the accuracy and the need for large tables of characteristic absorption lengths for each unique temperature profile.

The line limiting factor defined in (4) is one of the possible handlings of the line overestimation. The more traditional approach is based upon the so called '*escape factor*', which replaces the absorption coefficient of strong lines κ_{line} with $\kappa_{line}e^{-\kappa_{line}l}$, where l is some characteristic lengths [6]. It might be interesting to provide the comparison between the escape factor and line limiting provided by (4). Therefore, we modified the optimization process described in the previous section to accommodate the escape factor. The results of the process are shown in figure 5. Direct comparison with figure 4 reveals that there is practically no difference in the accuracy achievable by both methods with the line limiting according to (4) providing marginally better accuracy. However, the escape factor requires more precise estimation of characteristic length and loses accuracy much faster compared to the line limiting proposed by Nordborg. We therefore consider the line limiting according to (4) a superior option.
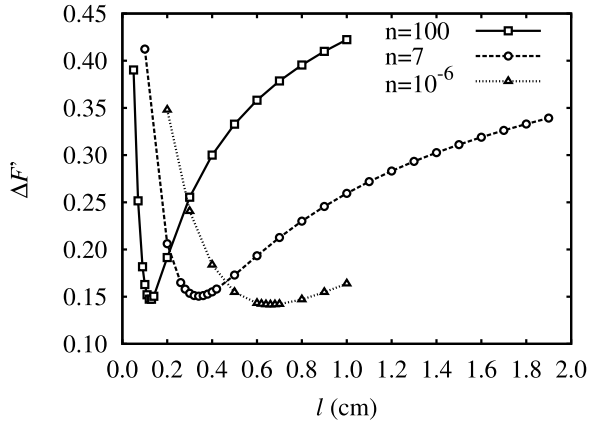
J. Phys. D: Appl. Phys. **50** (2017) 305201

P Kloc *et al*

Figure 5. Dependence of the reduced norm on the characteristic length *l* with an escape factor as line limiting mechanism.

3.2. Optimized mean absorption bands

We encountered several regions with unique band distributions during our calculations with varying characteristic absorption lengths. It does not make much sense to list all of them. Rather, it is more important to focus on the band distribution close to the best value L_{best} of the characteristic absorption length. We listed all the relative band distributions in table 2 including both the L_{best} and L_{optim} characteristic absorption lengths.

One can clearly see a repeated pattern here. Nearly all of the listed band distributions result in the same frequency boundaries, which holds even when the optimal characteristic absorption length of three plasma radii is considered. Temperature profiles with a core temperature of 10 kK are a notable exception here. Yet, it is hardly surprising because at this low temperature, the far UV parts of the spectra play far less of an important role compared to higher temperatures. The optimal band boundaries are therefore shifted to the lower frequencies, as confirmed by the tabulated values. This process is already visible at temperature profiles with a core temperature of 15 kK albeit to lesser extent.

Another important effect is the contribution of the molecular species to the absorption coefficient at low temperature. This effect would shift the optimal band distribution further away from those listed in table 2, increasing the error if such band limits were used instead.

A very wide range, at which one particular band distribution is applicable, makes us very confident in proposing it as the optimal three band distribution for air plasma at a pressure of 1 bar with a core temperature above 10 kK. The optimal band boundaries are summarized in the table 3 and shown relative to the spectral absorption coefficient at 25 kK on figure 6. Note that the position of optimal band boundaries correspond to the significant changes in the absorption continuum. More precisely, it corresponds to the photoionization edge of the ground state and the first excited state of nitrogen. The method of assigning the band boundaries to the changes in the absorption continuum used by many teams [4, 7, 10] can be considered good practise and is supported by our calculation, at least in the extent of a small number of bands and a line limited Planck MAC.

Table 2. Frequency of band boundaries of three bands approximation expressed in 10^{15} Hz. Band boundaries are listed for both cases of the characteristic absorption length L_{best} and $L_{optim} = 3R_p$ as indicated in the last column. Note that only the boundaries of the second (inner) band are listed. The frequency of other bands outer boundaries were fixed at $0.01 \cdot 10^{15}$ Hz and 10^{16} Hz for the first and the third band, respectively.

T_{max} (kK)	$n = 100$	$n = 7$	$n = 10^{-6}$	
25	3.0231–3.5130	2.9376–3.5130	2.9376–3.5130	L_{best}
25	3.0231–3.5130	2.9376–3.5130	2.9376–3.5130	L_{optim}
20	2.9150–3.5130	2.9376–3.5130	2.9376–3.5130	L_{best}
20	2.9150–3.5130	2.9376–3.5130	2.9376–3.5130	L_{optim}
15	2.9376–3.5130	2.9376–3.3968	2.9376–3.2111	L_{best}
15	2.9376–3.5130	2.9376–3.2844	2.9376–3.3476	L_{optim}
10	2.9376–3.4728	2.9376–3.2363	2.9376–3.0959	L_{best}
10	2.4335–2.9853	2.4898–3.0460	2.9376–3.0620	L_{optim}

Table 3. Band limits for three band approximation in air at pressure of 1 bar.

Band nr.	Limits (10^{15} Hz)
1	$0.001 – 2.93759$
2	$2.93759 – 3.51299$
3	$3.51299 – 10.0$
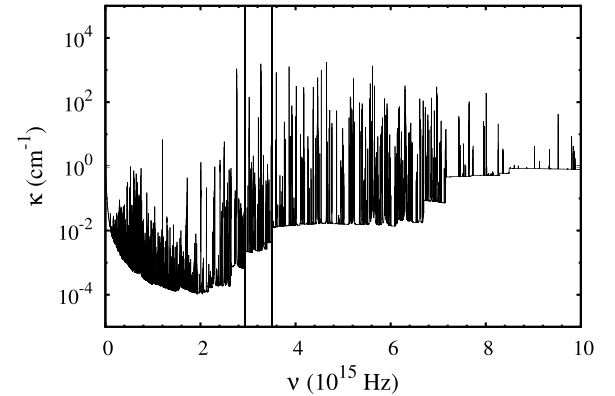
Figure 6. Absorption coefficient of air at 25 kK and position of optimal band boundaries.

The band boundaries specified in table 3 are subsequently used to calculate the MACs presented in the appendix of this paper (see tables A1 and A2).

3.3. Divergence of radiation flux

Knowing the overall accuracy can often be sufficient, but it is worth looking at the comparison of the divergence of radiation flux between the spectral and approximate solution in more detail. If there is any inherent inaccuracy in the deployment of MACs, it would be apparent on profiles of the divergence of the radiation flux. It would even be possible to compensate for known systematic errors in subsequent numerical calculations.

A comparison of the divergence of the radiation flux using both the spectral solution and approximation with MACs is shown in figures 7 and 8, respectively, for temperature profiles with core temperature 25 kK and 15 kK. Solid lines correspond
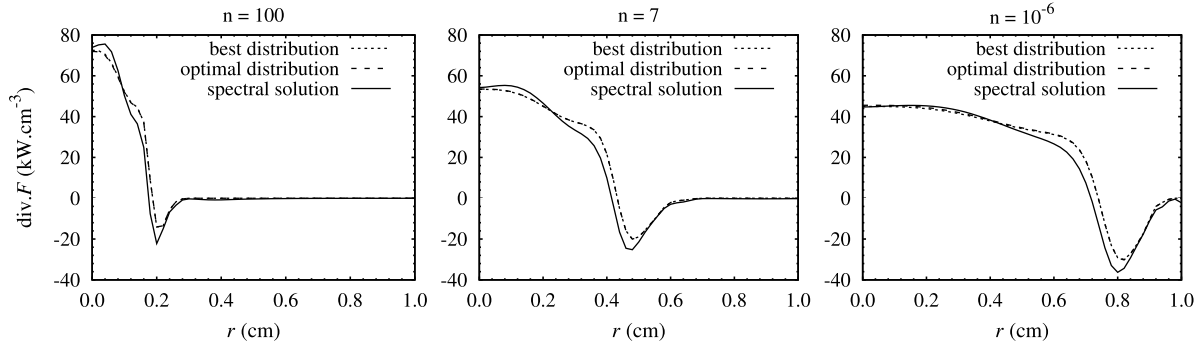
Figure 7. Divergence of radiation flux along the cylinder radius for various temperature profiles with core temperature 25 kK. Solid line calculated using spectrally resolved absorption coefficient. Dashed lines correspond to MACs with either L_{best} or L_{optim} in the line limiting factor and related band distribution.
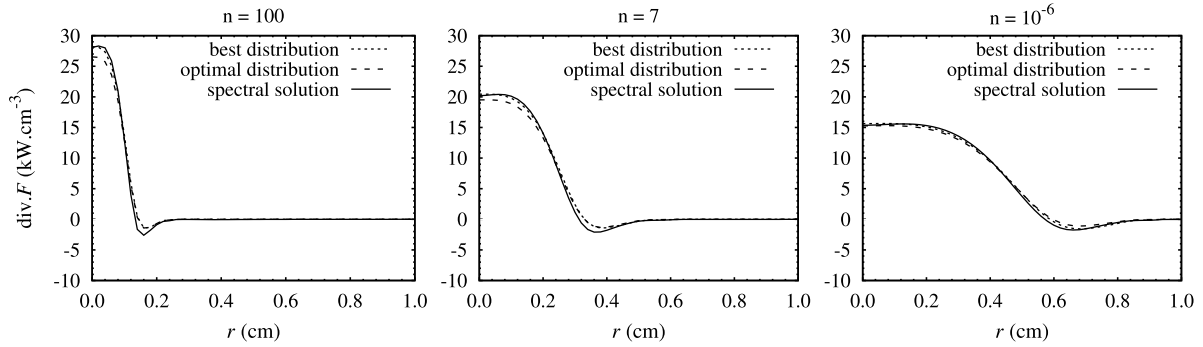
Figure 8. Divergence of radiation flux along cylinder radius for various temperature profiles with core temperature 15 kK. Solid line calculated using spectrally resolved absorption coefficient. Dashed lines correspond to MACs with either L_{best} or L_{optim} in the line limiting factor and related band distribution.
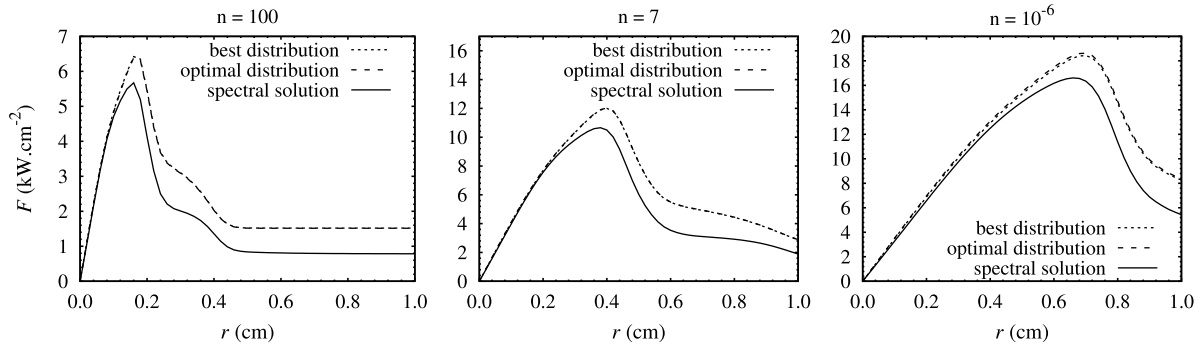
Figure 9. Radiation flux along cylinder radius for various temperature profiles with core temperature 25 kK. Solid line calculated using spectrally resolved absorption coefficient. Dashed lines correspond to MACs with either L_{best} or L_{optim} in the line limiting factor and related band distribution.

Figure 10. Radiation flux along cylinder radius for various temperature profiles with core temperature 15 kK. Solid line calculated using spectrally resolved absorption coefficient. Dashed lines correspond to MACs with either L_{best} or L_{optim} in the line limiting factor and related band distribution.

to the spectral solution, while dashed lines to the MACs approximation. The best solution (corresponding to L_{best} with band distribution from table 2) and optimal sol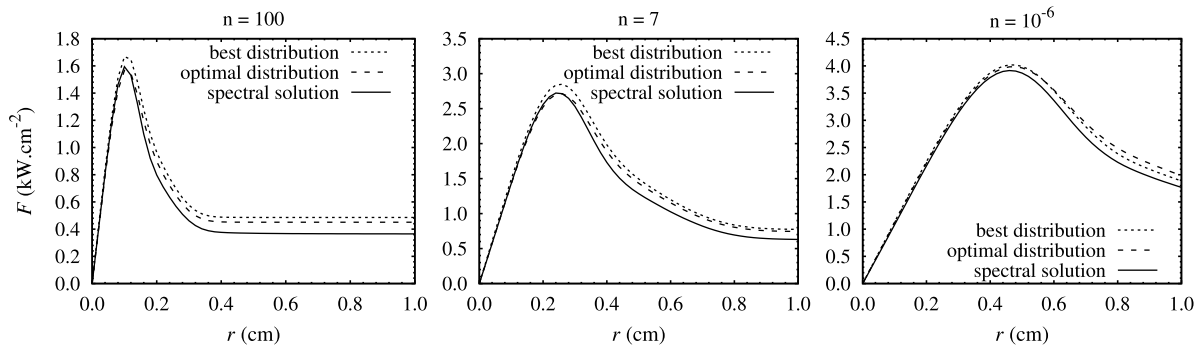ution (corresponding to $L_{optim} = 3R_p$ with the band distribution from table 3) closely overlap in the case of 25 kK. In the case of 15 kK, the situation is bit different where the optimal band distributions tend to underestimate the emission part by as much as 8% while the best solution provides a very good approximation. We consider this an acceptable accuracy given the number of bands.

Unfortunately, even a relatively small discrepancy in the divergence of radiation flux can greatly influence the accuracy of the radiation flux. This is clearly visible in figures 9 and 10, where the error of the mean absorption approximation reaches 50%. The radiation flux calculated via mean absorption coefficients overestimates the exact solution, especially in the outer parts of the plasma. This overestimation of the flux is clearly caused by the underestimation of the absorption visible on the divergence of the radiation flux profiles. One might expect that an improvement can be achieved by using radiation flux as the optimization objective function. Our testing shows that this might improve the radiation flux profile at the cost of divergence of radiation flux accuracy. In this paper, we focus on the radiation energy balance inside the plasma characterized by the divergence of the radiation flux and discussing other possible objective functions goes beyond the focus of this this paper.

Overall, the approximation using Planck MACs tends to underestimate the absorption at the outskirt of the plasma column. The error lingers around 15% and can go up to 20%. Unfortunately, it also means that the amount of radiation escaping the plasma and reaching the potential wall is rather overestimated. The cause of this is probably in the line limiting procedure itself, as radiation reabsorption by atomic lines plays an important role in the total radiation absorption. Increasing the number of bands would probably decrease the error but would not eliminate the problem entirely. A different approach to the calculation of the mean value inside each band might help, but more investigation in this area is needed.

4. Conclusion

This paper illustrates the method used to calculate the optimal mean absorption coefficient band distribution for radiation heat transfer in air at the pressure of 1 bar. This method is applicable to low voltage circuit breakers and switching devices, for example. The results suggest that it is possible to reach a very good approximation to the spectral solution with as few as three bands. The band distribution from table 3 is applicable to a very wide range of conditions and shows only marginally worse results compared to the best band distribution outside this range. The optimal band distribution seems to correspond to the changes in the absorption continuum. Calculations of the divergence of the radiation flux using the suggested band distribution tend to underestimate the absorption outside the plasma column while quite correctly predicting the value within the column.

Using Planck MAC requires proper treatment of atomic lines, which in turn needs knowledge of the characteristic absorption length L. We propose that the value of $L = 3R_p$ should be used, keeping in mind that it is much better to overestimate the value of the characteristic absorption length rather than underestimate it. Reliance on beforehand knowledge or estimation of plasma radius R_p is the greatest disadvantage of the proposed method.

We present the tables of mean Planck absorption coefficients for each band as a function of temperature and characteristic absorption length in the appendix. These tables can be used for the fast estimation of radiation transfer coupled with either DOM or P1 spatial approximation. The tabulated data are applicable to the air plasma with a pressure of 1 bar and a core temperature above 10 kK.

Acknowledgments

J. Phys. D: Appl. Phys. **50** (2017) 305201

P Kloc *et al*

Appendix. Tables of MAC for air at pressure of 1 bar

Table A1. Mean absorption coefficients of air.

	$L = 0.1$ mm			$L = 1.0$ mm		
T (K)	Band 1	Band 2	Band 3	Band 1	Band 2	Band 3
300	2.584×10^{-07}	8.105×10^{-05}	3.843×10^{-04}	2.584×10^{-07}	8.105×10^{-05}	3.777×10^{-04}
500	1.229×10^{-07}	3.684×10^{-05}	8.848×10^{-04}	1.229×10^{-07}	3.684×10^{-05}	3.930×10^{-04}
700	7.781×10^{-08}	4.704×10^{-05}	4.039×10^{-03}	7.781×10^{-08}	4.704×10^{-05}	1.277×10^{-03}
1000	4.936×10^{-08}	1.232×10^{-04}	1.339×10^{-02}	4.936×10^{-08}	1.232×10^{-04}	3.763×10^{-03}
2000	3.216×10^{-08}	4.952×10^{-03}	6.098×10^{-02}	3.216×10^{-08}	3.359×10^{-03}	1.740×10^{-02}
3000	1.541×10^{-06}	1.474×10^{-01}	5.647×10^{-01}	1.541×10^{-06}	2.800×10^{-02}	4.658×10^{-01}
4000	4.061×10^{-05}	3.406×10^{-01}	$2.228 \times 10^{+00}$	4.061×10^{-05}	8.454×10^{-02}	$2.007 \times 10^{+00}$
5000	1.197×10^{-04}	5.145×10^{-01}	$2.965 \times 10^{+00}$	1.196×10^{-04}	1.376×10^{-01}	$2.670 \times 10^{+00}$
6000	1.927×10^{-04}	7.189×10^{-01}	$4.974 \times 10^{+00}$	1.869×10^{-04}	2.227×10^{-01}	$4.658 \times 10^{+00}$
7000	3.224×10^{-04}	$1.036 \times 10^{+00}$	$8.771 \times 10^{+00}$	2.345×10^{-04}	4.212×10^{-01}	$8.470 \times 10^{+00}$
8000	9.264×10^{-04}	$1.378 \times 10^{+00}$	$1.064 \times 10^{+01}$	4.293×10^{-04}	6.718×10^{-01}	$1.035 \times 10^{+01}$
9000	2.635×10^{-03}	$1.685 \times 10^{+00}$	$1.032 \times 10^{+01}$	9.844×10^{-04}	8.792×10^{-01}	$1.003 \times 10^{+01}$
10 000	6.669×10^{-03}	$1.972 \times 10^{+00}$	$9.467 \times 10^{+00}$	2.435×10^{-03}	$1.045 \times 10^{+00}$	$9.166 \times 10^{+00}$
11 000	1.458×10^{-02}	$2.185 \times 10^{+00}$	$8.387 \times 10^{+00}$	5.512×10^{-03}	$1.151 \times 10^{+00}$	$8.074 \times 10^{+00}$
12 000	2.664×10^{-02}	$2.243 \times 10^{+00}$	$7.063 \times 10^{+00}$	1.045×10^{-02}	$1.167 \times 10^{+00}$	$6.747 \times 10^{+00}$
13 000	4.033×10^{-02}	$2.094 \times 10^{+00}$	$5.538 \times 10^{+00}$	1.645×10^{-02}	$1.082 \times 10^{+00}$	$5.229 \times 10^{+00}$
14 000	5.038×10^{-02}	$1.740 \times 10^{+00}$	$3.981 \times 10^{+00}$	2.153×10^{-02}	9.089×10^{-01}	$3.687 \times 10^{+00}$
15 000	5.246×10^{-02}	$1.282 \times 10^{+00}$	$2.637 \times 10^{+00}$	2.370×10^{-02}	6.929×10^{-01}	$2.359 \times 10^{+00}$
16 000	4.707×10^{-02}	8.550×10^{-01}	$1.666 \times 10^{+00}$	2.260×10^{-02}	4.864×10^{-01}	$1.403 \times 10^{+00}$
17 000	3.840×10^{-02}	5.434×10^{-01}	$1.059 \times 10^{+00}$	1.947×10^{-02}	3.227×10^{-01}	8.128×10^{-01}
18 000	3.021×10^{-02}	3.515×10^{-01}	7.144×10^{-01}	1.574×10^{-02}	2.088×10^{-01}	4.824×10^{-01}
19 000	2.407×10^{-02}	2.445×10^{-01}	5.273×10^{-01}	1.239×10^{-02}	1.364×10^{-01}	3.051×10^{-01}
20 000	2.010×10^{-02}	1.878×10^{-01}	4.283×10^{-01}	9.745×10^{-03}	9.302×10^{-02}	2.107×10^{-01}
21 000	1.787×10^{-02}	1.587×10^{-01}	3.770×10^{-01}	7.795×10^{-03}	6.818×10^{-02}	1.601×10^{-01}
22 000	1.686×10^{-02}	1.455×10^{-01}	3.523×10^{-01}	6.437×10^{-03}	5.464×10^{-02}	1.332×10^{-01}
23 000	1.662×10^{-02}	1.421×10^{-01}	3.428×10^{-01}	5.538×10^{-03}	4.754×10^{-02}	1.193×10^{-01}
24 000	1.682×10^{-02}	1.453×10^{-01}	3.420×10^{-01}	4.983×10^{-03}	4.387×10^{-02}	1.126×10^{-01}
25 000	1.722×10^{-02}	1.522×10^{-01}	3.453×10^{-01}	4.677×10^{-03}	4.204×10^{-02}	1.098×10^{-01}
26 000	1.761×10^{-02}	1.597×10^{-01}	3.486×10^{-01}	4.537×10^{-03}	4.106×10^{-02}	1.088×10^{-01}
27 000	1.780×10^{-02}	1.655×10^{-01}	3.486×10^{-01}	4.486×10^{-03}	4.037×10^{-02}	1.083×10^{-01}
28 000	1.766×10^{-02}	1.682×10^{-01}	3.434×10^{-01}	4.464×10^{-03}	3.972×10^{-02}	1.071×10^{-01}
29 000	1.705×10^{-02}	1.675×10^{-01}	3.321×10^{-01}	4.433×10^{-03}	3.900×10^{-02}	1.048×10^{-01}
30 000	1.595×10^{-02}	1.634×10^{-01}	3.151×10^{-01}	4.376×10^{-03}	3.817×10^{-02}	1.013×10^{-01}

Table A2. Mean absorption coefficients of air—continuation.

T (K)	$L = 10$ mm			$L = 100$ mm		
	Band 1	Band 2	Band 3	Band 1	Band 2	Band 3
300	2.584×10^{-07}	8.105×10^{-05}	3.754×10^{-04}	2.584×10^{-07}	8.102×10^{-05}	3.741×10^{-04}
500	1.229×10^{-07}	3.684×10^{-05}	2.444×10^{-04}	1.229×10^{-07}	3.683×10^{-05}	1.951×10^{-04}
700	7.781×10^{-08}	4.704×10^{-05}	4.880×10^{-04}	7.781×10^{-08}	4.704×10^{-05}	2.296×10^{-04}
1000	4.936×10^{-08}	1.232×10^{-04}	1.248×10^{-03}	4.936×10^{-08}	1.232×10^{-04}	4.490×10^{-04}
2000	3.216×10^{-08}	1.299×10^{-03}	8.857×10^{-03}	3.216×10^{-08}	5.863×10^{-04}	6.510×10^{-03}
3000	1.541×10^{-06}	6.780×10^{-03}	4.462×10^{-01}	1.541×10^{-06}	2.834×10^{-03}	4.418×10^{-01}
4000	4.061×10^{-05}	3.312×10^{-02}	$1.960 \times 10^{+00}$	4.061×10^{-05}	2.221×10^{-02}	$1.951 \times 10^{+00}$
5000	1.195×10^{-04}	6.462×10^{-02}	$2.606 \times 10^{+00}$	1.195×10^{-04}	5.036×10^{-02}	$2.593 \times 10^{+00}$
6000	1.847×10^{-04}	1.247×10^{-01}	$4.587 \times 10^{+00}$	1.839×10^{-04}	1.053×10^{-01}	$4.573 \times 10^{+00}$
7000	2.058×10^{-04}	2.894×10^{-01}	$8.400 \times 10^{+00}$	1.989×10^{-04}	2.617×10^{-01}	$8.386 \times 10^{+00}$
8000	2.885×10^{-04}	5.046×10^{-01}	$1.028 \times 10^{+01}$	2.441×10^{-04}	4.690×10^{-01}	$1.027 \times 10^{+01}$
9000	5.089×10^{-04}	6.691×10^{-01}	$9.961 \times 10^{+00}$	3.405×10^{-04}	6.235×10^{-01}	$9.946 \times 10^{+00}$
10 000	1.112×10^{-03}	7.852×10^{-01}	$9.090 \times 10^{+00}$	6.569×10^{-04}	7.270×10^{-01}	$9.075 \times 10^{+00}$
11 000	2.429×10^{-03}	8.456×10^{-01}	$7.996 \times 10^{+00}$	1.342×10^{-03}	7.746×10^{-01}	$7.981 \times 10^{+00}$
12 000	4.524×10^{-03}	8.315×10^{-01}	$6.669 \times 10^{+00}$	2.392×10^{-03}	7.504×10^{-01}	$6.653 \times 10^{+00}$
13 000	7.027×10^{-03}	7.408×10^{-01}	$5.151 \times 10^{+00}$	3.604×10^{-03}	6.553×10^{-01}	$5.135 \times 10^{+00}$
14 000	9.125×10^{-03}	5.902×10^{-01}	$3.611 \times 10^{+00}$	4.562×10^{-03}	5.077×10^{-01}	$3.595 \times 10^{+00}$
15 000	1.007×10^{-02}	4.227×10^{-01}	$2.287 \times 10^{+00}$	4.919×10^{-03}	3.498×10^{-01}	$2.271 \times 10^{+00}$
16 000	9.753×10^{-03}	2.806×10^{-01}	$1.337 \times 10^{+00}$	4.668×10^{-03}	2.203×10^{-01}	$1.321 \times 10^{+00}$
17 000	8.649×10^{-03}	1.803×10^{-01}	7.507×10^{-01}	4.067×10^{-03}	1.324×10^{-01}	7.351×10^{-01}
18 000	7.279×10^{-03}	1.166×10^{-01}	4.229×10^{-01}	3.394×10^{-03}	7.942×10^{-02}	4.076×10^{-01}
19 000	5.966×10^{-03}	7.746×10^{-02}	2.468×10^{-01}	2.792×10^{-03}	4.900×10^{-02}	2.318×10^{-01}
20 000	4.855×10^{-03}	5.317×10^{-02}	1.525×10^{-01}	2.310×10^{-03}	3.164×10^{-02}	1.376×10^{-01}
21 000	3.969×10^{-03}	3.782×10^{-02}	1.011×10^{-01}	1.941×10^{-03}	2.146×10^{-02}	8.597×10^{-02}
22 000	3.297×10^{-03}	2.807×10^{-02}	7.251×10^{-02}	1.668×10^{-03}	1.530×10^{-02}	5.692×10^{-02}
23 000	2.804×10^{-03}	2.186×10^{-02}	5.629×10^{-02}	1.471×10^{-03}	1.141×10^{-02}	4.009×10^{-02}
24 000	2.450×10^{-03}	1.787×10^{-02}	4.688×10^{-02}	1.336×10^{-03}	8.849×10^{-03}	3.004×10^{-02}
25 000	2.198×10^{-03}	1.532×10^{-02}	4.124×10^{-02}	1.245×10^{-03}	7.100×10^{-03}	2.386×10^{-02}
26 000	2.017×10^{-03}	1.364×10^{-02}	3.762×10^{-02}	1.185×10^{-03}	5.868×10^{-03}	1.989×10^{-02}
27 000	1.880×10^{-03}	1.247×10^{-02}	3.501×10^{-02}	1.139×10^{-03}	4.968×10^{-03}	1.715×10^{-02}
28 000	1.769×10^{-03}	1.157×10^{-02}	3.283×10^{-02}	1.091×10^{-03}	4.291×10^{-03}	1.508×10^{-02}
29 000	1.669×10^{-03}	1.080×10^{-02}	3.078×10^{-02}	1.034×10^{-03}	3.763×10^{-03}	1.336×10^{-02}
30 000	1.574×10^{-03}	1.013×10^{-02}	2.878×10^{-02}	9.649×10^{-04}	3.352×10^{-03}	1.183×10^{-02}

References

[1] Cressault Y, Takali S, Rohani V, Cauneau F and Fulcheri L 2015 *Proc. 21st Int. Conf. on Gas Discharges and their Applications (Nagoya) vol* 1 p 81

[2] Lowke J J 1974 *J. Quant. Spectrosc. Radiat. Transfer* **14** 111–22

[3] Aubrecht V and Lowke J J 1994 *J. Phys. D: Appl. Phys.* **27** 2066–73

[4] Randrianandraina H Z, Cressault Y and Gleizes A 2011 *J. Phys. D: Appl. Phys.* **44** 194012

[5] Modest M F 2013 *Radiative Heat Transfer* (Oxford: Academic) p 480

[6] Nordborg H and Iordanidis A A 2008 *J. Phys. D: Appl. Phys.* **41** 135205

[7] Peyrou B, Chemartin L, Lalande P, Cheron B G, Riviere P, Perrin M-Y and Soufiani A 2012 *J. Phys. D: Appl. Phys.* **45** 455203

[8] Jan C, Cressault Y, Gleizes A and Bousoltane K 2014 *J. Phys. D: Appl. Phys.* **47** 015204

[9] Reichert F, Gonzalez J-J and Freton P 2012 *J. Phys. D: Appl. Phys.* **45** 375201

[10] Hannachi R, Cressault Y, Salem D, Teulet P, Bejo L and Lakhdar Z B 2012 *J. Phys. D: Appl. Phys.* **45** 485206

[11] Fagiano L and Gati R 2016 *J. Quant. Spectrosc. Radiat. Transfer* **169** 58–78

[12] Kloc P, Aubrecht V, Bartlova M and Coufal O 2015 *J. Phys. D: Appl. Phys.* **48** 055208

[13] Coufal O 2007 *J. Phys. D: Appl. Phys.* **40** 3371

[14] Coufal O and Zivny O 2011 *Eur. Phys. J. D* **61** 131

[15] Whiting E E 1968 *J. Quant. Spectrosc. Radiat. Transfer* **8** 1379–84

[16] Kloc P, Aubrecht V, Bartlova M, Coufal O and Ruempler C 2015 *Plasma Chem. Plasma Process.* **35** 1097–110

[17] Changtong L and Bo Y 2012 *J. Glob. Optim.* **52** 45–55